Water oxidation electrocatalysis in acidic media with Fe-containing POMs/carbon composites‡

Khalid Azmani,[a,b] Maria Besora,[b] Jiahao Yu,[a] Anne-Lucie Teillout,[c] Pedro de Oliveira,[c] Israël-Martyr Mbomekallé,[c] Joaquín Soriano-López,[d] Josep M. Poblet,[b] José-Ramón Galán-Mascarós[a,e]**

[a]Institute of Chemical Research of Catalonia (ICIQ), The Barcelona Institute of Science and Technology (BIST), Av. Països Catalans, 16. Tarragona, E-43007, Spain.

[b]Departament de Química Física i Inorgànica, Universitat Rovira i Virgili, Marcel·lí Domingo 1, E-43007 Tarragona, Spain.

[c]Equipe d'Electrochimie et de Photo-électrochimie, Institut de Chimie Physique, UMR 8000, CNRS, Université Paris-Saclay, Orsay, F-91405, France

[d]Institut de Ciència Molecular, Universitat de València, Catedrático José Beltrán 2, 46980 Paterna, Spain.

[e]ICREA, Pg. Lluís Companys 23, 08010 Barcelona, Spain

‡This article is dedicated to the late Professor Achim Müller, whose unwavering commitment to science has inspired many of us to explore the frontiers of knowledge with enthusiasm and rigor

ABSTRACT. Iron-based catalysts are very appealing in terms of applications due to the low cost of Fe and to its abundance in the Earth's crust. In the field of water oxidation, unfortunately, iron oxides cannot match the activity of Co or Ni oxides, much less the activity of noble metal oxides (IrO_2). The activity of transition metals to promote the oxygen evolution reaction (OER) can be tuned and enhanced by their incorporation into polyoxometalate frameworks (POMs). In comparison with metal oxides, POMs offer a controlled, discrete structure, and a tailor-made environment. Fe-POMs still show a low OER activity in neutral or basic media, when compared to Co-POMs. When moving to highly acidic media, we have found an unexpected electrochemical response in carbon paste electrodes containing salts of the $[Fe^{III}_4(H_2O)_2(PW_9O_{34})2]^{6-}$ (**Fe_4**) polyanion. In oxidative conditions, these electrodes showed lower onset potentials, and higher current densities than their Co-based analogs, contrary to computational expectations. Careful analyses have shown the excellent stability of the **Fe_4** in these pH < 1 conditions, but a poor selectivity. CO_2 is the dominant product, in addition to O_2. The capability of **Fe_4** to oxidize amorphous carbon in acidic conditions appears to be unique, since it is not found in Fe oxides or simple Fe salts. Thus, Fe-POMs, in acidic conditions, are still modest OER catalysts, but exhibit a unique performance when electrochemically oxidizing carbon.

Introduction

Polyoxometalates (POMs) are a wide family of molecular fragments of metal oxides built from MO_x polyhedral of early transition metal cations in high oxidation states. Thanks to their discreet and well-defined structure,[1] along their chemical and redox stability in multiple solvents, they have been model materials of study in multiple fields, from supramolecular chemistry[2,3] to molecular magnetism,[4,,6] from bio-inorganic activity[7] to nanoscience.[8,9] A major application of POMs deals with their catalytic activity, in homogeneous and heterogeneous conditions.[10,,,13] This catalytic

activity is based in two of their most prominent features: their acid-base and their redox capabilities, taking and donating protons or electrons, respectively. [14,,16] In the last decade they have been investigated as model catalysts to accelerate (photo)electrochemical reactions,[17] with promising performance in water electrolysis.[18 - 27]

Hydrogen production from water electrolysis powered by renewable energy sources has been identified as a key contributor to the desired decarbonization of the industry worldwide.[28] Electrolytic hydrogen is still limited by different challenges, one of them being the sluggish kinetics and high overpotential of the oxygen evolution reaction (OER) at the anode.[29] This is particularly difficult in acidic media, given the poor stability of common OER electrocatalysts (transition metal oxides) in such electrolytes.[30] After decades of research, IrO_2-based catalysts are still the only ones providing fast enough kinetics and viable long-term stability.[31] Thus, many research and technology initiatives are looking for cost-effective, earth-abundant alternatives.

One highly successful strategy to stabilize active OER electrocatalysts in acidic media comes from surface engineering of common metal oxides to provide a distinct surface that favors water-hydroxyl trapping,[32] and offering good stability at high current densities. Some other promising strategies have been successful only at low current densities. For instance, by limiting the applied potential to avoid the dissolution of the active species.[33 -36] The processing of OER catalysts into a partially hydrophobic/conducting support is also able to avoid acid attack.[37,38] With the latter strategy, Co-POMs demonstrated to be highly active and robust towards OER even in 1M H_2SO_4 electrolyte with good stability in comparison with IrO_2.[39] It is also relevant to mention that this solid composite electrode with insoluble POM salts is particularly appealing, since POMs are typically unstable as homogeneous catalysts for OER.[40,41]

Motivated by its abundancy and innocuous character, iron is the most interesting transition metal to be explored as water oxidation catalyst. But in terms of activity, iron offers modest performance towards OER. This was confirmed with oxides,[42] and also with Fe-POMs. The $[Fe^{III}_4(H_2O)_2(PW_9O_{34})_2]^{6-}$ (**Fe$_4$**) polyanion (**Fig. 1**)[43,44] exhibited lower OER kinetics than the analogous $[Co^{II}_4(H_2O)_2(PW_9O_{34})_2]^{10-}$ (**Co$_4$**) POM in neutral pH.[45-47] These results were corroborated by computational modelling, which concluded that the transition state in the Fe-POM was energetically more demanding due to the different electronic features.

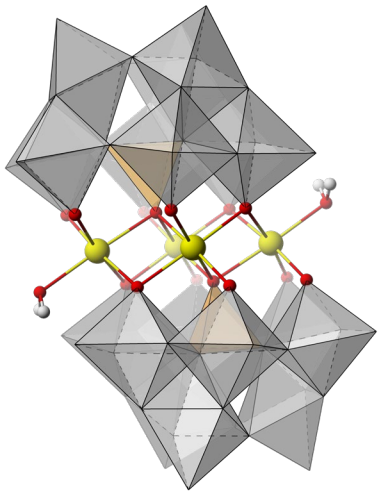

Figure 1. Molecular structure of the $[M_4(H_2O)_2(PW_9O_{34})_2]^{n-}$ polyanions. Sandwich-type polyoxometalates based on two B-α-$[XW_9O_{34}]^{q-}$ (X = P^V, As^V, Si^{IV}) and four transition metal centers constitute a well-known class of compounds.

Despite being a less active catalyst, we decided to investigate the activity of **Fe$_4$** for OER also in acidic media. Surprisingly, we have found a significant lower onset potential and better electrochemical activity in the Fe *vs* Co species comparison, contrary to what was observed in neutral pH. **Fe$_4$** exhibits excellent structural and chemical stability in these conditions. However, this electrocatalytic performance is not coming exclusively from the OER process, with a major

side reaction: carbon oxidation to CO_2. This activity is unprecedented, and still not well understood, appearing as a unique reactivity of Fe-POMs for the oxidation of amorphous carbon.

Methods

Materials. All chemicals and solvents were used as purchased without further purification. Milli-Q water (ca. 18.2 MΩ·cm resistivity) was employed to prepare all aqueous solutions and to clean and rinse the electrodes. Carbon paste (CP) was purchased from ALS (CPO Carbon Paste Oil: uniform-sized graphite powder and paraffin oil).

Electrode preparation. The CP blends were prepared by mixing the barium salts of the POMs with CP in the desired weight ratios using an agate mortar. Then, the blend was introduced into the CP electrode pocket. A small piece of staple cotton was used to cover the electrode surface for long-term electrocatalytic experiments to avoid the expulsion of the blend out of the electrode pocket.

Electrochemical methods. All electrochemical experiments were performed using a Biologic SP150 potentiostat. Ohmic drop was compensated (85%) using the positive feedback compensation implemented in the instrument. All experiments were performed with a three-electrode configuration using a glass H-cell, with a glass frit separating the cathode chamber from the anode chamber. The pocket of the CP electrode (surface area = 0.07 cm^2) was the working electrode, and the Saturated Calomel Electrode (SCE) was the reference electrode, both placed in the anode compartment. A Pt mesh was used as counter electrode in the cathode compartment. Linear sweep voltammetry experiments (LSV) were performed at scan rate of 1 mV/s. Bulk water electrolysis was performed at a constant current density of 1 mA/cm^2 for 2–24h. All current densities were calculated based on the geometrical surface area of the electrodes (0.07 cm^2).

The experiments were carried out in an H_2SO_4 (1 M) aqueous solution at pH ≈ 0.3. The actual pH of the electrolyte was measured prior to each experiment, and the thermodynamic potential for the water oxidation was corrected by the pH value using the Nernst equation:

$$E^0 = 1.229 - (0.059 \times \mathrm{pH})\ (\mathrm{V})\ \text{vs NHE at } 25\ ^\circ\mathrm{C}$$

The water oxidation overpotentials (η) were calculated by subtracting the thermodynamic water oxidation potential to the applied potential:

$$\eta = E_{app} - E^{0}_{H_2O/O_2}$$

Recovery of the catalyst. After electrochemical experiments, the Ba[POM]/CP blend (ca. 40 mg) was suspended in acetone (30 mL) and sonicated for 30 minutes. The supernatant liquid (containing carbon black and the organic oil binder) was decanted to retain the POM catalyst in the beaker. This procedure was repeated ten times to get a clean catalyst sample, ready for post-catalytic characterization.

Characterization methods. IR spectra were collected with a FT-IR Bruker spectrometer model Alpha equipped with an ATR accessory. The spectra were acquired in the range 400–4000 cm^{-1} with 32 scans. Raman measurements were acquired using a Renishaw inVia Reflex Raman confocal microscope (Gloucester- Shire, UK), equipped with a diode laser emitting at 785 nm at a nominal power of 300 mW, and a Peltier-cooled CCD detector (−70 ºC) coupled to a Leica DM-2500 microscope. Calibration was carried out by recording the Raman spectrum of an internal Si standard. Rayleigh scattered light was appropriately rejected by using edge-type filters. The spectra were acquired in the range 100–1800 cm^{-1}. Laser power was used at nominal 1% to avoid sample damage. Spectra were recorded with the accumulation of at least three scans with a 30 s scan time each one.

Computational methods: The methodology used follows our recent analysis on the OER activity of **Fe$_4$** in neutral media.[45] Optimizations were performed using the Gaussian-16 package,[48] with the B3LYP hybrid functional[49,50,51] and simulating the solvent effects of water using the IEF-PCM[52] model (ε = 78.36 and UFF radii). As basis sets, the 6-31G(d,p)[53,54,55] were used for all light atoms whereas for P, W and Fe atoms the LANL2DZ effective core potential (ECP)[56] was used instead. The nature of all stationary points was verified by computation of the vibrational frequencies. All energies reported correspond to the computed free Gibbs energies in solution; electrochemical steps are reported either in V or eV and chemical steps in eV and kcal mol^{-1}. All experimental and computed potentials and overpotentials given in the present work are referred to the NHE reference scale. A collection data set of all computational data is accessible in the ioChem-BD repository.[57]

Results and discussion

Electrochemical characterization

The insoluble $Ba_3[Fe^{III}_4(H_2O)_2(PW_9O_{34})_2]$ salt (**BaFe$_4$**) was blended with a carbon paste to produce solid conducting electrodes up to a 30% POM content in weight (**x-Fe$_4$/CP**). The electrochemical response of these **x-Fe$_4$/CP** composites was studied in 3-elecrode configuration in 1M H_2SO_4 electrolyte (pH < 0.3), with a Pt mesh counter-electrode and a Saturated Calomel (SCE) reference electrode. The linear sweep voltammetry data showed the onset of an oxidation event at very low potentials, with increasing activities as the POM content increases (**Fig. 2**). Comparing these results with analogous **Co$_4$** electrodes, **Fe$_4$** offers an apparent better performance (higher current densities at a given overpotential), contrary to our observations in neutral pH.[45] Chronopotentiometry also showed a good stability in the **20-Fe$_4$/CP** electrodes for > 10 hours (**Fig. 3**).

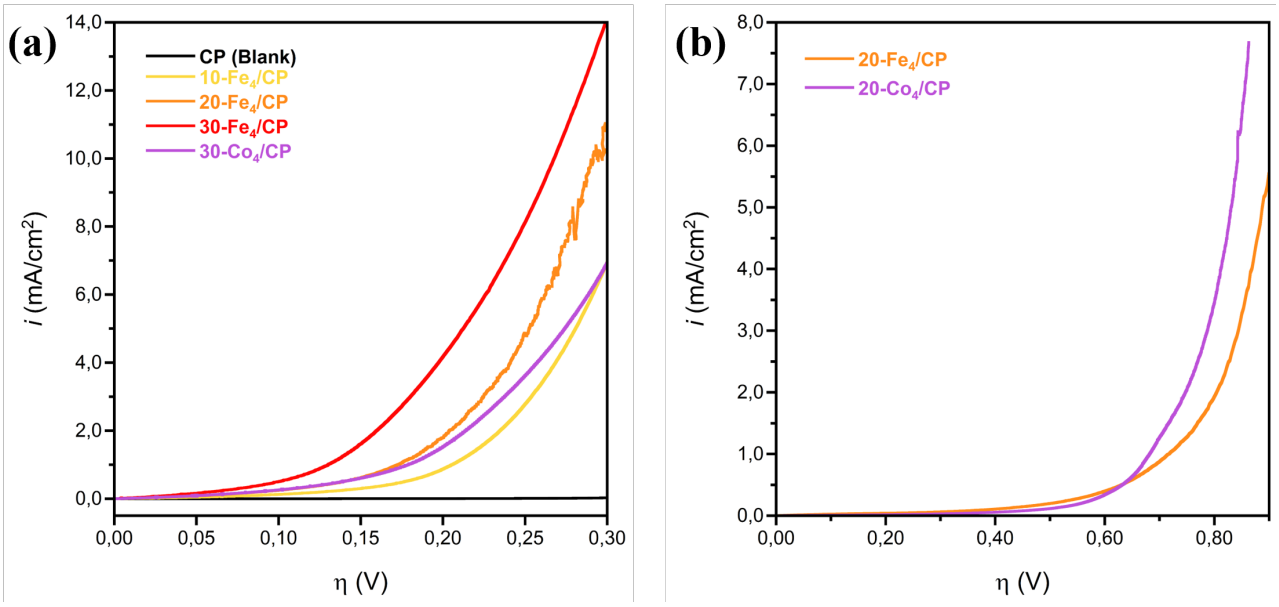

Figure 2. Linear sweep voltammetry (LSV, 1 mV/s) of **Fe$_4$** and **Co$_4$** carbon paste electrodes in 1 M H_2SO_4 electrolyte (pH < 0.3) (a) and in phosphate pH 7 buffer (b).

During chronopotentiometry, we analyzed the head space of the anode with a fluorescent probe to quantify the oxygen evolution. Multiple and reproducible experiments gave a surprisingly low oxygen yield, reaching a maximum of ≈ 30 % O_2 of the theoretically expected production (**Fig. 4a**). Although the detection of O_2 in these conditions is challenging, given the small surface area of the electrode, and the plausible trapping of O_2 into the carbon paste, such a low efficiency was unexpected, far from the > 95% efficiency toward OER shown by Fe_4/CP electrodes in neutral media,[45] and also the >99% efficiency towards OER obtained for the analogous **Co_4** in acidic conditions.[39]

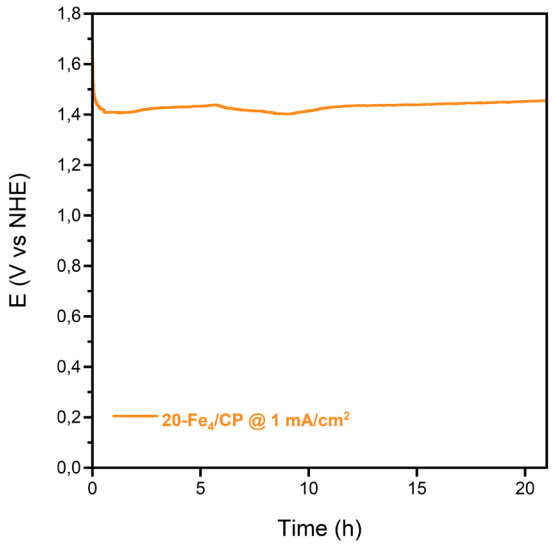

Figure 3. Chronopotentiometry at 1 mA/cm^2 of 20-Fe_4/CP electrodes in 1 M H_2SO_4 electrolyte.

To identify additional products, given the low Faradaic efficiency towards water oxidation, we built a set-up (Figure S1) to analyze the gas evolution during chronopotentiometry with a mass spectrometry (MS) instrument, using argon as carrier gas. The set-up consists of a hermetic H-cell with two compartments. After 16 h of chronopotentiometry, the Ar flow was passed through the anode head space and into the MS analyzer. The results showed two major components in the gas stream, O_2 and also CO_2. Although MS makes it difficult to accurately quantify their exact ratio,

given the MS specifications, CO_2 is clearly the major product considering the MS response areas (**Fig. 4b**). The gas diffusion dynamics of CO_2 and O_2 are not comparable in the Ar gas stream, with most oxygen being detected in the first 2 hours, while CO_2 detection continues for > 4 hours, always once the chronopotentiometry has been stopped (before flowing Ar through the cell). From the total integration of the signal a rough 4:1 ratio between CO_2 and O_2 can be estimated. No other volatile compounds were detected by the MS.

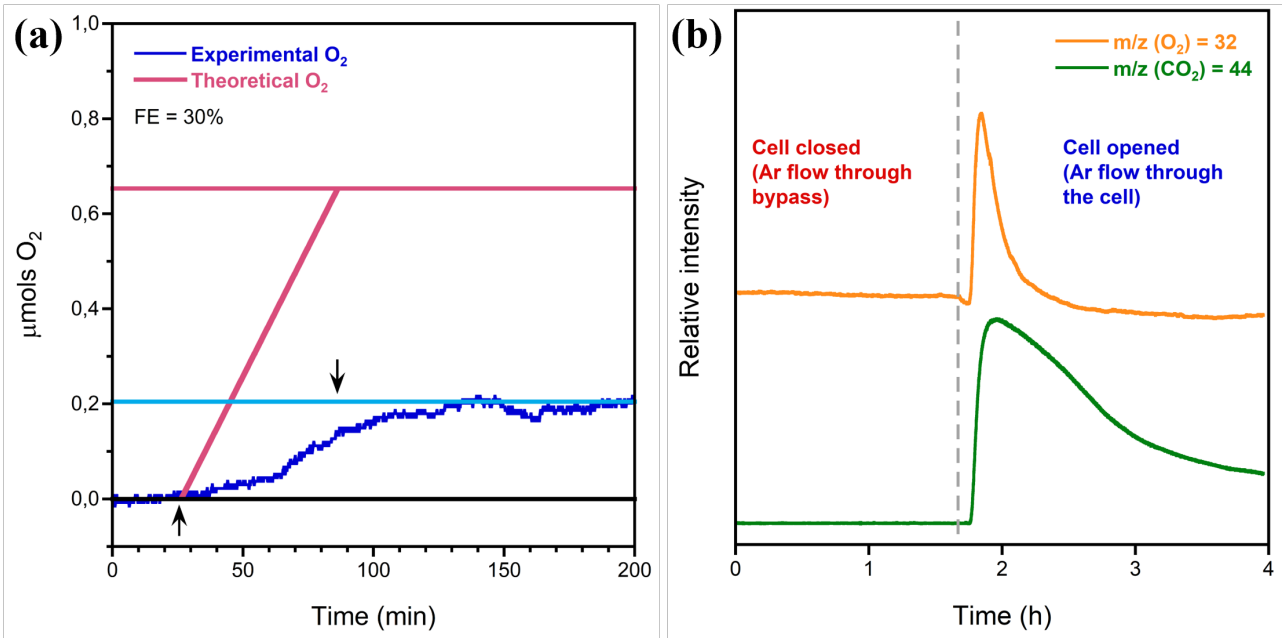

Figure 4. (a) Experimental and theoretical oxygen evolution during a chronopotentiometry experiment at 1 mA/cm^2 of 20-Fe$_4$/CP electrodes in 1 M H_2SO_4 electrolyte. The arrow indicates the chronopotentiometry starting and ending points. Faradaic efficiency (FE) remains at 30%. (b) O_2 and CO_2 detection after 16 hours of chronopotentiometry experiment at 1 mA/cm^2 of 20-Fe$_4$/CP electrodes in 1 M H_2SO_4 electrolyte. The dashed line indicates when the chronopotentiometry stops, and an Ar stream starts to flow through the cell directing the headspace gas to the mass spectroscopy analyzer.

The most plausible origin for CO_2 should be the amorphous carbon in the carbon paste composite, since it is the only carbon source in the system. To understand if this activity is unique for the Fe-POMs, we investigated the activity of carbon paste composites containing iron sulfate, as an alternative Fe^{3+} compound. CO_2 evolution was not detected with this salt, which showed very poor

electrochemical response in the same voltage range (Figure S2). Fe oxides in CP electrodes for OER in acidic conditions were already reported, and no activity towards CO_2 evolution detected.[37] Thus, this capability to oxidize amorphous carbon appears to be a special feature of the Fe-POMs.

Post-chronopotentiometry characterization

The stable chronopotentiometry data (> 10 h) suggests good **Fe_4/CP** stability during acidic OER. To further assess the robustness of the **Fe_4**, we recovered the electrode composite along the mother liquor after the chronopotentiometry for further analyses. ICP-OES carried out with the mother liquor of the anode compartment confirmed the absence of any metal, beyond the detection limit (Table S1). Raman and IR spectroscopy of the composite electrodes do not show any significant changes in the main signature peaks of the **Fe_4** species (Figure S3). The IR shows some additional peaks at ~1600 cm^{-1}, due to the presence of carbon residues. The fingerprint of the **Fe_4** species in the 1200-500 cm^{-1} is well-match, with minor variations in peak resolution, which improves after catalysis (probably because of the different hydration, due to the multiple acetone washes to remove the carbon content). The Raman shows no new peaks, as expected to detect any transformation or decomposition of the POM structure.[58,59]. All these data suggest a good stability of the catalyst during acidic electrooxidations in these composite electrodes.

Computational Studies

The reaction mechanism for the water oxidation with **Fe_4** was previously studied in neutral media.[45] In that study, the Fe^{III}-OH_2 species evolved to iron-hydroxy species Fe^{III}-OH and from there the postulated mechanism involved Fe^{II}/Fe^{IV} intermediates with a potential determining step of 1.54 V corresponding to the PCET between Fe^{III}-OH and Fe^{IV}=O. Herein, we compare the

results for the acidic media with those of the neutral media (see Computational Details). The species involved in the mechanism in acidic media are not the same, as in acidic media the starting species is not the iron-hydroxy Fe^{III}-OH, but the corresponding aqua complex Fe^{III}-OH_2. In Figure 6 the initial steps are presented, whereby vertical processes correspond to oxidation reactions (electron transfer, ET), horizontal ones to proton transfer (PT) and diagonal arrows represent proton coupled electron transfer (PCET) steps with one electron and one proton loss. Fe^{III}-OH_2 needs 2.5 eV to undergo a PCET to form the corresponding iron-hydroxy complex Fe^{IV}-OH, and from that point it can evolve to {H}Fe^{IV}=O and Fe^{IV}=O. {H}Fe^{IV}=O is the result of an internal rearrangement of the hydroxylic hydrogen to protonate an oxo group of the POM, whereas Fe^{IV}=O is the result of the spontaneous loose of a proton leading to Fe^{IV}=O.

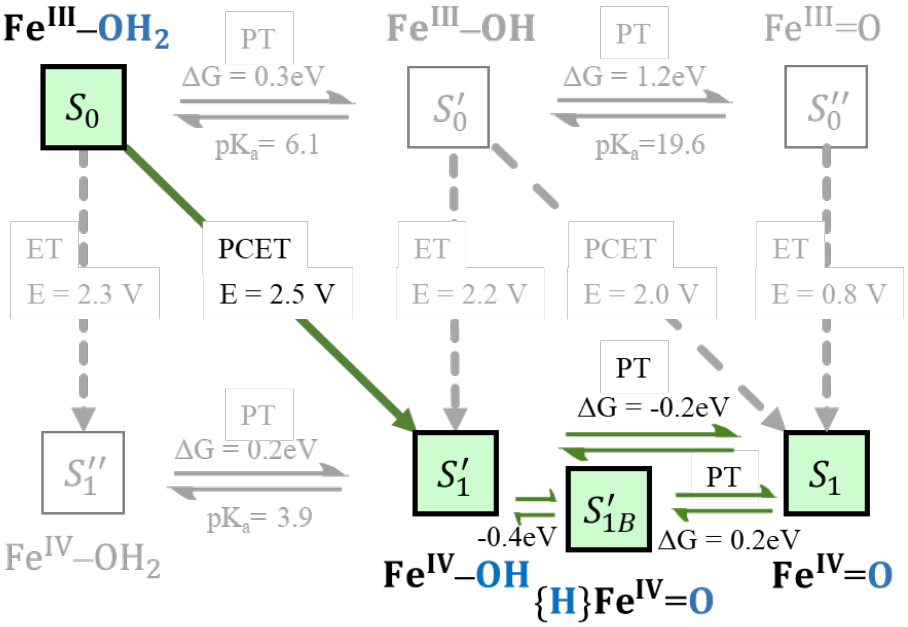

Figure 6. Diagram representation of the PCET, PT and ET events for Fe_4 at pH = 0 to reach the *active* species. Potentials are given in V vs NHE for the electrochemical processes, while the chemical processes related to acid-base equilibria (PT) are expressed as free Gibbs energy (in eV).

Further analyzing the square diagram, we can see that from the starting species, Fe^{III}-OH_2, another similar mechanism is possible, in which the iron aqua species Fe^{III}-OH_2 is in acid-base equilibria with Fe^{III}-OH. In acidic media a small proportion of Fe^{III}-OH would be available and could undergo a PCET with a potential of 2.0V to achieve Fe^{IV}=O. This mechanism, although lower in the required potential, would not be very efficient due to the low concentration of starting species.

Once the Fe^{IV}=O species is formed, the subsequent steps in acidic media closely resemble those observed in neutral media. However, the reaction requires larger potentials in acidic conditions due to the higher proton concentration, which hinders proton release as described by the Nernst equation. Computational analysis indicates that a potential over 2.0 V is necessary for oxygen evolution, a value significantly higher than experimental observations. These results suggest that oxygen evolution efficiency under acidic conditions is likely low. Further experimental and computational studies are needed to completely understand the reaction mechanism and accurately reproduce the effect of the acidic environment.

Conclusions

The use of a carbon-based, hydrophobic electrode support is able to stabilize water oxidation catalysts in acidic media, avoiding their dissolution at high proton concentrations. This has been also confirmed in the case of the **Fe_4** polyoxometalate. **Fe_4**/carbon paste electrodes are able to sustain an anodic current in 1 M H_2SO_4 electrolyte for hours, confirming the high stability of the **Fe_4** species under these conditions. However, product analyses have shown a high production of CO_2, suggesting the contribution of carbon oxidation to the observed currents.

This is the first example of the carbon support oxidation during water oxidation with these composite electrodes, since Faradaic oxygen evolution was found for all other OER catalysts, including POMs and also transition metal oxides in previous studies.[37,38,39] Even the very same **Fe$_4$** showed Faradaic OER in neutral media, indicating a major role of the acidic environment to promote carbon oxidation.[45] This finding may open interesting opportunities for electrochemical carbon oxidation, with Fe-POMs appearing as plausible catalysts for biomass electrochemical decomposition.

ASSOCIATED CONTENT

Supporting Information.

The following files are available free of charge.

Additional characterization data and analysis (PDF)

AUTHOR INFORMATION

Corresponding Authors

*joaquin.soriano@uv.es; jrgalan@iciq.es

Notes

The authors declare no competing interests.

ACKNOWLEDGMENT

The authors acknowledge the financial support from MCIN/AEI/10.13039/501100011033 through projects PID2021-124796OB-I00 and PID2023-149905NB-I00; and from the Generalitat de Catalunya (grants 2021SGR1154 and 2021SGR00110). ICIQ is supported by the Ministerio de

Ciencia e Innovacion through the Severo Ochoa Excellence accreditation CEX2021-001214- S; and by the CERCA Pro-gramme/Generalitat de Catalunya. A.-L.T., P.d.O. and I.-M.M. thank the Université Paris-Saclay and the CNRS for financial support. M. B thanks the grant CNS2022-136079 funded by MICIU/AEI/ 10.13039/501100011033 and by the "European Union NextGenerationEU/PRTR. J.S.-L. acknowledges the funding from Generalitat Valenciana thought the Plan Gen-T of Excellence (CDEIGENT/2021/037).

REFERENCES

(1) Cronin, L.; Müller, A. From serendipity to design of polyoxometalates at the nanoscale, aesthetic beauty and applications. *Chem. Soc. Rev.* **2012**, *41*, 7333–7334.

(2) Liu, T. B.; Diemann, E.; Li, H. L.; Dress, A. W. M.; Müller, A. Self-assembly in aqueous solution of wheel-shaped Mo_{154} oxide clusters into vesicles. *Nature* **2003**, *426*, 59–62.

(3) Wang, Y.; Weinstock, I. A. Polyoxometalate-decorated nanoparticles. *Chem. Soc. Rev.* **2012**, *41*, 7479–7496.

(4) Bertaina, S.; Gambarelli, S.; Mitra, T.; Tsukerblat, B.; Müller, A.; Barbara, B. Quantum oscillations in a molecular magnet. *Nature* **2008**, *453*, 203–206.

(5) Kortz, U.; Müller, A.; van Slageren, J.; Schnack, J.; Dalal, N. S.; Dressel, M. Polyoxometalates: Fascinating structures, unique magnetic properties. *Coord. Chem. Rev.* **2009**, *253*, 2315–2327.

(6) Clemente-Juan, J. M.; Coronado, E.; Gaita-Ariño, A. Magnetic polyoxometalates: from molecular magnetism to molecular spintronics and quantum computing. *Chem. Soc. Rev.* **2012**, *41*, 7464–7478.

(7) Rhule, J. T.; Hill, C. L.; Judd, D. A. Plyoxometalates in medicine. *Chem. Rev.* **1998**, *98*, 327–357.

(8) Müller, A.; Beckmann, E.; Bögge, H.; Schmidtmann, M.; Dress, A. Inorganic chemistry goes protein size: A Mo_{369} nano-hedgehog initiating nanochemistry by symmetry breaking. *Angew. Chem. Int. Ed.* **2002**, *41*, 1162–1163.

(9) Ji, Y. C.; Huang, L. J.; Hu, J.; Strec, C.; Song, Y. F. Polyoxometalate-functionalized nanocarbon materials for energy conversion, energy storage and sensor systems. *Energy Environ. Sci.* **2015**, *8*, 776–789.

(10) Proust, A.; Matt, B.; Villanneau, R.; Guillemot, G.; Gouzerh, P.; Izzet, G. Functionalization and post.functionalization: a step towards polyoxometalate-based materials. *Chem. Soc. Rev.* **2012**, *41*, 7605–7622.

(11) Izarova, N. V.; Pope, M. T.; Kortz, U. Noble metals in polyoxometalates. *Angew. Chem. Int. Ed.* **2012**, *51*, 9492–9510.

(12) Weinstock, I. A.; Schreiber, R. E.; Neumann, R. Dioxygen in polyoxometalate mediated reactions. *Chem. Rev.* **2018**, *118*, 2680–2717.

(13) Zhang, Z. F.; Zhai, Y. H.; Gu, M. N.; Lei, H. T.; Li, Y. X.; Li, Y.; Tian, Y. Y., Zhu, G. S. Ionic porous aromatic frameworks embedding polyoxometalates for heterogeneous catalysis. *Chem. Eur. J.* **2024**, *30*, e202400796.

(14) Cai, L. X.; Li, S. C.; Yan, D. N.; Zhou, L. P.; Guo, F.; Sun, Q. F. Water-soluble redox-active cage hosting polyoxometalates for selective desulfurization catalysis. *J. Am. Chem. Soc.* **2018**, *140*, 4869–4876.

(15) Horn, M. R.; Singh, A.; Alomari, S.; Goberna-Ferron, S.; Benages-Vilau, R.; Chodankar, N.; Motta, N.; Ostrikov, K.; MacLeod, J.; Sonar, P.; Gomez-Romero, P.; Dubal, D. Polyoxometalates (POMs): from electroactive clusters to energy materials. *Energy Environ. Sci.* **2021**, *14*, 1652–1700.

(16) Liu, G. F.; Zhang, S.; Chen, C. J.; Xing, S. M.; Zhang, X. Y.; Zhang, Y. J.; Wu, D. Y.; Li, J. F.; Ren, B.; Chen, J. J. Electrochemical hydrogenation of nitrobenzene: From electrocatalysis to redox mediator catalysis. *Chem. Mater.* **2024**, *36*, 8825–8833.

(17) Walsh, J.J.; Bond, A. M.; Forster, R. J.; Keyes, T. E. Hybrid polyoxometalate materials for photo(electro-)chemical applications. *Coord. Chem. Rev.* **2016**, *306*, 217–234.

(18) Sartorel, A.; Bonchio, M.; Campagna, S.; Scandola, F. Tetrametallic molecular catalysts for photochemical water oxidation. *Chem. Soc. Rev.* **2013**, *42*, 2262–2280.

(19) Matt, B.; Fize, J.; Moussa, J.; Amouri, H.; Pereira, A.; Artero, V.; Izzet, G.; Proust, A. Charge photo-accumulation and photocatalytic hydrogen evolution under visible light at an iridium(iii)-photosensitized polyoxotungstate. *Energy Environ. Sci.* **2013**, *6*, 1504–1508.

(20) Streb, C. New trends in polyoxometalate photoredox chemistry: From photosensitization to water oxidation catalysis. *Dalton Trans.* **2012**, *41*, 1651–1659.

(21) Geletii, Y. V.; Besson, C.; Hou, Y.; Yin, Q.; Musaev, D. G.; Quiñonero, D.; Cao, R.; Hardcastle, K. I.; Proust, A.; Kogeler, P.; Hill, C. L. Structural, physicochemical, and reactivity properties of an all-inorganic, highly active tetraruthenium homogeneous catalysts for water oxidation. *J. Am. Chem. Soc.* **2009**, *131*, 17360–17370.

(22) Sartorel, A.; Carraro, M.; Scorano, G.; De Zorzi, R.; Geremia, S.; McDaniel, N. D.; Bernhard, S.; Bonchio, M. Poluyoxometalate embedding of a tetraruthenium(IV)-oxo-core by template-directed metalation of $[\gamma\text{-}SiW_{10}O_{36}]^{8-}$: A totally inorganic oxygen-evolving catalyst. *J. Am. Chem. Soc.* **2008**, *130*, 5006–5007.

(23) Toma, F. M.; Sartorel, A.; Lurio, M.; Carraro, M.; Parisse, P.; Maccato, C.; Rapino, S.; Rodríguez-Gonzalez, B.; Amenitsch, H.; Da Ros, T.; Casalls, L.; Goldoni, A.; Mascaccio, M.; Scorrano, G.; Scoles, G.; Paolucci, F.; Prato, M.; Bonchio, M. Efficient water oxidation at carbon nanotube-polyoxometalate electrocatalytic interfaces. *Nat. Chem.* **2010**, *2*, 826–831.

(24) Sakthinathan, I.; Köhling, J.; Wagner, V.; McCormac, Y. Layer-by-layer construction of a nanoarchitecture by polyoxometalates and polymers: Enhanced electrochemical hydrogenb evolution reaction. *ACS Appl. Mater. Interfaces* **2023**, *15*, 2861–2872.

(25) Zeb, Z.; Huang, Y.; Chen, L.; Zhou, W.; Liao, M.; Jiang, Y.; Li, H.; Wang, L.; Wang, L.; Wang, H.; Wei, T.; Znag, D.; Fan, Z.; Wei, Y. Comprehensive overview of polyoxometalates for electrocatalytic hydrogen evolution reaction. *Coord. Chem. Rev.* **2023**, *482*, 215058.

(26) Zhao, M.; Liu, Q.; Feng, Y.; Lv, H. Recent advances in polyoxometalate-based catalysts for light-driven hydrogen evolution. *Dalton Trans.* **2024**, advanced article. doi: 10.1039/D4DT02357A

(27) Dashtian, K.; Shahsavarifar, S.; Usman, M.; Jospeh, Y.; Ganjali, M. R.; Yin, Z.; Rahimi-Nasrabadi, M. A comprehensive review on advanced in polyoxometalate based materials for electrochemical water splitting. *Coord. Chem. Rev.* **2024**, *504*, 215644.

(28) Vartiainen, E.; Breyer, C.; Moser, D.; Medina, E. R.; Busto, C.; Masson, G.; Bosch, E.; Jäger-Waldau, A. True cost of solar hydrogen, *Sol. RRL* **2021**, 2100487.

(29) Xie, X.; Du, L.; Yan, L.; Park, S.; Qiu, Y.; Sokolowski, J.; Wang, W.; Shao, Y. Oxygen evolution reaction in alkaline environment: Materials challenges and solutions. *Adv. Funct. Mater.* **2022**, *32*, 2110036.

(30) McCrory, C. C L.; Jung, S.; Ferrer, I. M.; Chatman, S. M.; Peters, J. C.; Jaramillo, T. F. Benchmarking hydrogen evolving reaction and oxygen evolving reaction electrocatalysts for solar water devices. *J. Am. Chem. Soc.* **2015**, *137*, 4347–4357.

(31) Seitz, L. C.; Dickens, C. F.; Nishio, K.; Hikita, Y.; Montoya, J.; Doyle, A.; Kirk, C.; Vojvodic, A.; Hwang, H. Y.; Norskov, J. K.; Jaramillo, T. F. A highly active and stable IrOx/SrIrO3 catalyst for the oxygen evolution reaction. *Science* **2016**, *353*, 1011–1014.

(32) Ram, R. ; Xia, L.; Benzidi, H.; Guha, A.; Golovanova, V.; Garzón Manjón, A.; Llorens Rauret, D.; Sanz Berman, P.; Dimitropoulos, M.; Mundet, B.; Pastor, E.; Celorrio, V.; Mesa, C. A.; Das, A. M.; Pinilla-Sánchez, A.; Giménez, S.; Arbiol, J.; López, N.; García de Arquer, F. P.Water-hydroxide trapping in cobalt tungstate for proton Exchange membrane water electrolysis. *Science* **2024**, *384*, 1373–1380.

(33) Huang, J.; sheng, H.; Ross, R. D.; Han, J.; Wang, X.; Song, B.M Jin, S. Modifying redox properties and local bonding of Co_3O_4 by CeO_2 enhances oxygen evolution catalysis in acid. *Nat. Commun.* **2021**, *12*, 3036.

(34) Li, A.; Ooka, H.; Bonnet, N.; Hayashi, T.; Sun, Y.; Jiang, Q.; Li, C.; Han, H.; Nakamura, R. Stable potential windows for long-term electrocatalysis by manganese oxides under acidic conditions. *Angew. Chem. Int. Ed.* **2019***, 58*, 5054–5058.

(35) Zhang, B.; Zheng, X.; Voznyy, O.; Comin, R.; Bajdich, M.; García-Melchor, M.; Han, L.; Xu, J.; Liu, M.; Zheng, L.; García de Arquer, F. P.; Dinh, C. T.; Fan, F.; Yuan, M.; Yassitepe, E.; Chen, N.; Regier, T.; Liu, P.; Li, Y.; de Luna, P.; Janmohamed, A.; Xin, H. L.; Yang, H.; Vojvodic, A.; Sargent, E. H. Homogeneously dispersed multimetal oxygen-evolving catalysts. *Science* **2016***, 352,* 333–337.

(36) Wang, N.; Ou, P.; Miao, R. K.; Chang, Y.; Wang, Z.; Hung, S.; Abed, J.; Ozden, A.; Chen, H.; Wu, H.; Huang, J. E.; Zhou, D.; Ni, W.; Fan, L.; Yan, Y.; Peng, T.; Sinton, D.; Liu, Y.; Liang, H.; Sargent, E. H. Doping shortens the metal/metal distance and promotes OH coverage in non-noble acidic oxygen evolution reaction catalysts. *J. Am. Chem. Soc.* **2023**, *145*, 7829–7836.

(37) Yu, J.; Garcés-Pineda, F. A.; González-Cobos, J.; Peña-Díaz, M.; Rogero, C.; Giménez, S.; Spadaro, M. C.; Arbiol, J.; Barja, S.; Galan-Mascaros, J.R. Sustainable oxygen evolution electrocatalysis in aqueous 1 M H_2SO_4 with earth abundant nanostructured Co_3O_4. *Nat. Commun.* **2022**, *13*, 4341.

(38) Yu, J.; Giancola, S.;Khezri, B.;Nieto-Castro, D.; Redondo, J.; Schiller, F.; Barja, S.; Spadaro, M. C.; Arbiol, J.; Garcés-Pineda, F. A.; Galan-Mascaros, J.R. A survey of Earth-abundant metal oxides as oxygen evolution electrocatalysts in acidic media (pH < 1) *EES Catal.* **2023**, *1*, 765–773.

(39) Blasco-Ahicart, M.; Soriano-López, J.; Carbó, J. J.; Poblet, J. M.; Galan-Mascaros, J. R. Polyoxometalate electrocatalysts based on earth-abundant metals for efficient water oxidation in acidic media. *Nat. Chem.***2018**, *10*, 24–30.

(40) Folkman, S. J.; Soriano-Lopez, J.; Galan-Mascaros, J. R.; Finke, R. G. Electronically driven water-oxidation catalysis beginning with six exemplary cobalt polyoxometalates: Is it molecular, homogeneous catalysis or electrode-bound, heterogeneous CoO_x catalysis? *J. Am. Chem. Soc.* **2018**, *140*, 12040–12055.

(41) Rotonnelli, B.; Lassalle-Kaiser, B.; Bonnefont, A.; Renaudineau, S.; , Garnier, D.; Proust, A.; Bournel, F.; Gallet, J.-J.; Asset, T.; Savinova, E. Instability of cobalt substituted polyoxometalates during the oxygen evolution reaction: An operando X-ray absorption spectroscopy study. *J. Phys. Chem. C* **2024**, *128*, 7968–7976.

(42) Nguyen, H. C.; Garcés-Pineda, F. A.; De Fez-Febré, M.; Galan-Mascaros, J. R.; López, N. Non-redox doping boosts oxygen evolution electrocatalysis on hematite. *Chem. Sci* **2020**, *11*, 2464.

(43) Weakley, T. J. R.; Evans, H. T. jun.; Showell, J. S.; Tourné, G. F.; Tourné, C. M. 18-Tungstotetracobalto(II)diphosphate and related anions: a novel structural class of heteropolyanions. *J. Chem. Soc., Chem. Commun*. **1973**, 139–140.

(44) Finke, R. G.; Droege, M.; Hutchinson, J. R.; Gansow, O. Trivacant heteropolytungstate derivatives: the rational synthesis, characterization, and tungsten-183 NMR spectra of $P_2W_{18}M_4(H_2O)_2O_{68}^{10-}$ (M = cobalt, copper, zinc). *J. Am. Chem. Soc.***1981**, *103*, 1587–1589.

(45) Azmani, K.; Besora, M.; Soriano-López, J.; Landolski, M.; Teillout, A.-L.; de Oliveira, P.; Mbomekallé, I.-M.; Poblet, J. M.; Galan-Mascaros, J. R. Understanding polyoxometalates as water oxidation catalysts through iron *vs.* cobalt reactivity. *Chem. Sci.* **2021**, *12*, 8755–8766.

(46) Yin, Q.; Tan, J. M.; Besson, C.; Geletii, Y. V.; Musaev, D. G.; Kuznetsov, A. E.; Luo, Z.; Hardcastle, K. I.; Hill, C. L. A Fast Soluble Carbon-Free Molecular Water Oxidation Catalyst Based on Abundant Metals**.** *Science* **2010**, *328*, 342–345.

(47) Soriano-López, J.; Steuber, F. W.; Mulahmetović, M.; Besora, M.; Clemente-Juan, J. M.; O'Doherty, M.; Zhu, N.-Y.; Hill, C. L.; Coronado, E.; Poblet, J. M.; Schmitt, W. Accelerating water oxidation – a mixed Co/Fe polyoxometalate with improved turnover characteristics. *Chem. Sci.* **2023**, *14*, 13722-13733.

(48) Frisch, M. J.; Trucks, G. W.; Schlegel, H. B.; Scuseria, G. E.; Robb, M. A.; Cheeseman, J. R.; Scalmani, G.; Barone, V.; Petersson, G. A.; Nakatsuji, H.; Li, X.; Caricato, M.; Marenich, A. V.; Bloino, J.; Janesko, B. G.; Gomperts, R.; Mennucci, B.; Hratchian, H. P.; Ortiz, J. V.; Izmaylov, A. F.; Sonnenberg, J. L.; Williams-Young, D.; Ding, F.; Lipparini, F.; Egidi, F.; Goings, J.; Peng, B.; Petrone, A.; Henderson, T.; Ranasinghe, D.; Zakrzewski, V. G.; Gao, J.; Rega, N.; Zheng, G.; Liang, W.; Hada, M.; Ehara, M.; Toyota, K.; Fukuda, R.; Hasegawa, J.; Ishida, M.; Nakajima, T.; Honda, Y.; Kitao, O.; Nakai, H.; Vreven, T.; Throssell, K.; Montgomery, J. A., Jr.; Peralta, J. E.; Ogliaro, F.; Bearpark, M. J.; Heyd, J. J.; Brothers, E. N.; Kudin, K. N.; Staroverov, V. N.; Keith, T. A.; Kobayashi, R.; Normand, J.; Raghavachari, K.; Rendell, A. P.; Burant, J. C.; Iyengar, S. S.;

Tomasi, J.; Cossi, M.; Millam, J. M.; Klene, M.; Adamo, C.; Cammi, R.; Ochterski, J. W.; Martin, R. L.; Morokuma, K.; Farkas, O.; Foresman, J. B.; Fox, D. J. Gaussian 16, Revision B.01, Gaussian, Inc., Wallingford CT, 2016.

(49) Lee, C.; Yang, W.; Parr, R.G.; *Phys. Rev. B*, **1988**, *37*, 785–789.

(50) Becke, A.D.; *J. Chem. Phys*., **1992**, *96*, 2155–2160.

(51) Stephens, P. J.; Devlin, F. J.; Chabalowski, C. F.; Frisch, M. J.; *J. Phys. Chem.* **1994**, *98*, 11623–11627.

(52) Cancès, E.; Mennucci, B.; Tomasi, J.*; J. Chem. Phys.*, **1997**, *107*, 3032–3041.

(53) Francl, M. M.; Pietro, W. J.; Hehre, W. J.; Binkley, J. S.; Gordon, M. S.; DeFrees, D. J.; Pople, J. A.; *J. Chem. Phys.*, **1982**, *77*, 3654–3665.

(54) Hehre, W. J.; Ditchfield, R.; Pople, J.A.; *J. Chem. Phys*., **1972**, *56*, 2257–2261.

(55) Hariharan, P. C.; Pople, J. A.*; Theor. Chim. Acta*, **1973**, *28*, 213–222.

(56) Hay, P.J.; Wadt, W.R.; *J. Chem. Phys*., **1985**, *82*, 270–283.

(57) Álvarez-Moreno, M.; de Graaf, C.; López, N.; Maseras, F.; Poblet J. M.; C. Bo; *J. Chem. Inf. Model.*, **2015**, *55*, 95–103.

(58) Güttinger, R.; Wiprächtiger, G.; Blacque, O.; Patzke, G. R. *RSC Adv.* **2021**, *11*, 11425–11436.

(59) Cui, L.; Wang, Y.; Yu, K.; Ma, Y.; Zhou, B. *Adv. Funct. Mater.* **2024**, *34*, 2408968.

SYNOPSIS

A change in water oxidation catalytic selectivity is observed with Fe_4-modified carbon paste electrodes from neutral medium, displaying Faradaic O_2 evolution, to acidic conditions, in which the oxidation of the carbon support leads to the evolution of CO_2 and a reduction of the O_2 efficiency down to 30%. This unparalleled result may open new avenues for biomass electrochemical decomposition.